Biomaterials 74 (2016) 42–52

Contents lists available at ScienceDirect

Biomaterials

journal homepage: www.elsevier.com/locate/biomaterials

Directed cell growth in multi-zonal scaffolds for cartilage tissue engineering

Sandra Camarero-Espinosa [a, **], Barbara Rothen-Rutishauser [a], Christoph Weder [a], E. Johan Foster [a, b, *]

[a] Adolphe Merkle Institute, University of Fribourg, Chemin des Verdiers 4, 1700 Fribourg, Switzerland
[b] Virginia Tech, Macromolecules and Interfaces Institute, Virginia Tech Center for Sustainable Nanotechnology, Department of Materials Science & Engineering, 445 Old Turner Street, 213 Holden Hall, Blacksburg, VA 24061, USA

ARTICLE INFO

Article history:
Received 9 June 2015
Received in revised form
22 September 2015
Accepted 23 September 2015
Available online 28 September 2015

Keywords:
Cartilage
Scaffold
Tissue-engineering
Multi-layer
Nanocomposite

ABSTRACT

Articular cartilage serves as a low-friction cushion in synovial joints and is vital for mammalian skeletal movements. Due to its avascular nature and the low cell density, the tissue has a limited ability to regenerate, and damage due to injury, wear and tear, or disease usually requires surgical intervention. While articular cartilage had been predicted to be one of the first tissues to be successfully engineered, it proved to be challenging to reproduce the complex architecture and biomechanical properties of the native tissue. Here we report the fabrication of multi-layer polymer nanocomposite scaffolds that mimic the structural design, chemical cues, and mechanical characteristics of mature articular cartilage. These scaffolds guide the morphology, orientation, and phenotypic state of cultured chondrocytes in a spatially controlled manner, support the growth of tissue with features that are reminiscent of the natural analogue, and promote localized hydroxyapatite formation to permit integration with the subchondral bone.

1. Introduction

Adult articular cartilage was thought to be a straightforward target for tissue engineering, due to its avascular character and the fact the that only one cell type (chondrocytes) is present [1,2]. However, mature cartilage is composed of three distinct layers or zones, which vary in extra cellular matrix (ECM) components and cell phenotype, and the orientation of the constituents (Fig. 1) [3,4]. This structural complexity is the origin of the anisotropic, nonlinear viscoelastic mechanical properties of mature cartilage, which are largely governed by the zone-dependent orientation of collagen fibers and the osmotic pressure that is generated through the retention of synovial fluid via interactions with glycosaminoglycans (GAGs) [5].

On account of the demanding biomechanical environment of articular joints – large shear and compressive forces as well as high strains – successful tissue restoration requires the use of biomechanically robust cartilage regenerates [1,6,7]. It appears that this requirement can be better satisfied by *in-vitro* grown scaffold–neocartilage constructs, in which the artificial template initially provides adequate mechanical support [8,9], than by scaffold-less engineered cartilage replacements [10,11]. The specific structure, mechanical characteristics, and chemical environment of the scaffold can, in principle, also promote cell adhesion, proliferation, and differentiation and thereby guide tissue formation [12] and integration with the surrounding native tissue [13] and the subchondral bone [14].

In-vitro cell culture of articular chondrocytes has in many cases led to cell dedifferentiation and the formation of fibrocartilage, due to the absence of adequate chemical cues [15]. Scaffolds based on naturally derived hydrogels [16] or various synthetic polymeric scaffolds [8,9,12,17] have been shown to support the development of cartilage tissue with characteristic spherical chondrocyte morphology and phenotype, but due to their simplified structure their mechanical behavior is different from that of mature hyaline cartilage [18,19]. Stratified scaffolds which mimic the bone-

* Corresponding author. Virginia Tech, Macromolecules and Interfaces Institute, Virginia Tech Center for Sustainable Nanotechnology, Department of Materials Science & Engineering, 445 Old Turner Street, 213 Holden Hall, Blacksburg, VA 24061, USA.
** Corresponding author.
E-mail addresses: sandra.camareroespinosa@unifr.ch (S. Camarero-Espinosa), johanf@vt.edu (E.J. Foster).

http://dx.doi.org/10.1016/j.biomaterials.2015.09.033
0142-9612/

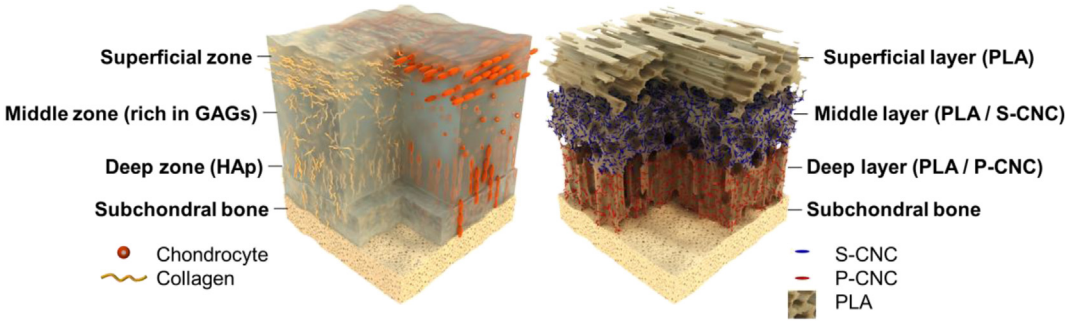

Fig. 1. Architecture of mature articular cartilage and the multi-layer polymer nanocomposite scaffolds studied. The simplified schematic representation shows the multi-zonal nature of native cartilage (left), in which cell morphology and phenotypic state, nature of extra cellular matrix components such as collagen and glycosaminoglycans (GAGs), and the orientation of some of these constituents are strongly dependent on the location. This architecture is mimicked by a porous multilayer scaffold (right) assembled from an anisotropic PLA superficial layer with tubular pores oriented parallel to the subchondral bone, an isotropic middle layer based on PLA and sulfated CNCs, and an anisotropic deep layer comprising PLA and phosphated CNCs with tubular pores oriented orthogonal to the subchondral bone.

cartilage interface and feature a bone-integrating phase and an isotropic cartilage phase [14], and multilayer scaffolds that emulate the graded mechanical properties of articular cartilage have recently been reported, the latter involving either density gradients [20] or a combination of porous layers with varying porosity and pore size [21,22]. While more complex scaffolds that closely mimic the multilayer structure and orientation of cartilage components, i.e. collagen and chondrocytes, and chemical cues associated with pertinent cell differentiation processes have recently been proposed as pathway to generate tissue constructs that are reminiscent of mature cartilage, such architectures have thus far not been realized [23].

We here report a multilayer polymer nanocomposite scaffold that mimics the distinct collagen orientation and ECM components of mature articular cartilage (Fig. 1). The new scaffold is comprised of three layers, which correspond to the superficial zone, middle zone, and deep zone of the native tissue. They were designed to guide the morphology, orientation, and phenotypic state of cultured chondrocytes in a spatially controlled manner, foster the integration with the subchondral bone, and provide adequate mechanical support.

2. Materials and methods

2.1. Extraction of phosphated and sulfated cellulose nanocrystals

Whatman filter paper No 1 was hydrolysed with sulfuric [24] or phosphoric acid [25] as described previously. Cellulose nanocrystals were then characterized by transmission electron microscopy (Supporting information Fig. S2) and conductometric titration (Supporting information Fig. S1) [25]. Aspect ratios of 8.7 ± 2.8 and 8.6 ± 2.1 were determined for sulfated and phosphated CNCs, respectively. The charge density of S–CNC and P–CNC was determined to be 98.5 ± 8.2 and 10.1 ± 1.6 mM/kg, respectively.

2.2. Rhodamine functionalized cellulose nanocrystals

Whatman filter paper No 1 was hydrolysed with hydrochloric acid following a slightly modified protocol [25] initially described by *Araki* et al. [26] These uncharged nanocrystals were sonicated 4 h in dry dimethylformamide at a 4% wt/wt concentration. 0.05 Equivalents of rhodamine B isothiocyanate (Sigma–Aldrich) and a drop of dibutyltindilaurate (Sigma–Aldrich) were added to the dispersion that was then stirred overnight at 100 °C under N_2 atmosphere. The dispersion was cleaned with 5 repetitions of centrifugation at 5000 rpm for 10 min in ethanol, decanting the supernatant and addition of fresh ethanol. The CNCs were then dialyzed against water for five days in the dark and freeze–dried. Functionalization was quantified by UV/Vis absorption spectroscopy at 555 nm and after baseline subtraction following standard addition procedure. The amount of rhodamine attached was determined to be 9.6 ± 0.3 mmol/kg of cellulose (Supporting information Fig. S5). Dimensions of rhodamine-CNCs were also characterized by transmission electron microscopy were an aspect ratio of 8.6 ± 2 was determined (Supporting information Fig. S6).

2.3. Scaffold fabrication

Poly(D,L-lactide) (D:L ratio 89:11) was purchased from NatureWorks (4060D) and used as received. A molecular weight (M_w) of 1.143×10^5 and a polydispersity (M_w/M_n) of 1.66 were calculated by standard gel permeation chromatography (GPC) experiments. Scaffolds were prepared by thermally induced phase separation (TIPS) as already described [27,28]. Isotropic scaffolds were prepared by solid–liquid TIPS from a 50 mg/mL polymer solution in a 1,4-dioxane: water mixture (87: 13, vol. %). 7.5 g of polymer were initially dissolved in 130.5 mL of 1,4-dioxane at room temperature under vigorous stirring overnight and 19.5 mL of water (non-solvent) were subsequently added to achieve a final polymer concentration of 50 mg/mL. When required, S–CNCs were added to reach a 10% wt./vol. ratio, and sonicated for 2 h in a sonication bath (Sonoswiss SW3H, Sonoswiss AG, Ramsen, Switzerland) adapted with continuous water flow to avoid heating of the sample. The solution was then heated to 60 °C for 1 h to overcome the cloud point of the mixture, creating an emulsion of water in the polymer/1,4-dioxane solution, which was then transferred to a plastic beaker and frozen in liquid nitrogen. After 1 h, to ensure complete freezing, polymer/solvent mixture blocks of around 9 cm diameter and 3–4 cm height (depending on the initial volume) were obtained and transferred to glass lyophilisation tanks that were immediately immersed in an ethylene glycol containing cooling bath at −10 °C (Julabo F25, Julabo GmBH, Seelbach, Germany). Flasks were then attached to a vacuum line operating at 10^{-2} torr and the sublimate was collected in a trap that was emptied twice per day until the sample was completely dry (3–4 days, depending on the starting volume). Anisotropic scaffolds were prepared in a similar fashion by a liquid–liquid TIPS method. Polymer solutions were prepared in dimethyl carbonate by combining 3.75 g of polymer with 150 mL of the solvent and stirring 4 h at room temperature to reach a concentration of 25 mg/mL. When required, P–CNCs were added to the solution and sonicated as described above to reach a 10% wt./vol. ratio. Dispersions were then transferred to a plastic beaker that

was immersed 1 h in liquid nitrogen. Frozen blocks were then transferred to glass lyophilisation tanks that were then immersed in an ethylene glycol cooling bath at −10 °C, and vacuum dried at 10^{-2} torr as explained above. Dry scaffold layers were punched with 8 mm diameter disposable biopsy punchers (Robbins Instruments Inc., NJ, USA).

Multi-layered scaffolds were prepared by gently wetting the surface of one of the layers with a dust free tissue paper impregnated with acetone (volatile solvent for the polymer) and bring it into contact with a second layer. The same process was repeated to attach the third layer.

2.4. Hydroxyapatite growth

Single scaffold layers consisting of neat isotropic and anisotropic PLA, PLA/P–CNC (anisotropic) and PLA/S–CNC (isotropic) were cut into cylindrical shapes of 8 mm diameter and 3–4 mm height (as measured with the caliper) with a disposable biopsy puncher and a razor blade. Samples were prepared in triplicate and place into 50 mL sterile centrifuge tubes that were filled up with a saturated $CaCl_2$ solution (100 mM) in ultrapure water (ρ = 18.2 mΩ cm). Samples were kept at 37 °C in an oven during the entire process. The solution was changed once per day for three days when samples were transferred to new 50 mL centrifuge tubes after rinsing with ultrapure water. Samples were then exposed to 1.5× simulated body fluid (11.994 g NaCl, 0.525 g $NaHCO_3$, 0.336 g KCl, 0.261 g K_2HPO_4, 0.458 g $MgCl_2{\cdot}6H_2O$, 60 mL HCl (1M), 0.417 g $CaCl_2$, 0.107 g Na_2SO_4, 9.086 g Tris $(CH_2OH)_3CNH_2$, in a total volume of 1 L of ultrapure water, pH 7.4). The solution was changed once per day for 7 days, when samples were transferred to Petri dishes and dried in the oven overnight at 50 °C.

2.5. Scanning electron microscopy (SEM) and energy dispersive X-ray scattering (EDX)

For morphological and compositional studies, the scaffolds were cut longitudinally and the inner faces were analyzed. Samples were mounted onto metallic supports with conductive double sided carbon tape. The perimeter of the porous samples was coated with silver conductive paint to ensure conductivity from the sample surface to the support (Auromal®). After a minimum of 1 h drying at room temperature samples were left overnight in high vacuum (10^{-6} atm) and coated afterwards with a gold (morphological experiments) or carbon (compositional experiments) layer. Sputtering of carbon (20–30 nm) was carried out on a Baltec CED 030 (Leica microsystems GmbH, VD, Switzerland). Gold sputtering was carried out in a Baltec MED 020 (Leica microsystems GmbH, VD, Switzerland). The thickness of the coating (25 nm) was simultaneously measured on an implemented quartz crystal microbalance.

Samples were analyzed on a SEM FEI XL30 Sirion FEG equipped with a secondary electron detector and a through the lenses detector (TLD) and a Centauros scintillator type backscattered electron detector equipped with a cathodoluminescent tip. The energy dispersive X-ray spectrometer system (EDAX Inc., NJ, USA) had a lithium doped silicon detector. Secondary electron micrographs were recorded under a voltage of 10 KeV with a spot size of 4–5 and a working distance of 10–20 mm. Backscattered electron micrographs were recorded under a voltage of 5 KeV with a spot size of 4 and a working distance of 5–10 mm. EDS spectra were recorded under a voltage of 25 KeV, a spot size of 4 and a working distance <5 mm. Spectra analysis was performed with a EDAX Genesis software version 5.2 with spectrum analysis, after automatic background subtraction, element peaks were identified and the ratio between elements was automatically determined.

2.6. Mechanical tests

Compression tests were carried out on a Zwick/Roell Z010 tensile tester equipped with 200 N and 10 kN load cells that were used for equilibrium and non-equilibrium tests, respectively. Experiments were carried out in PBS at a controlled temperature of 37 °C and continuous flow on a BioBath Environmental Chamber T 200 (TestResources). A preload of 5 and 25 kPa was applied to anisotropic and isotropic samples, respectively. Compression tests were carried out at a strain rate of 0.04 mm/min in all the experiments. Equilibrium creep tests were carried out by applying 16 steps of load with a controlled strain increase of 5% with 600 s relaxation time between steps. Young's and aggregate modulus were calculated from curves of 10 steps at a controlled strain rate of 1.5% with 600 s relaxation time between steps (Supporting information Figs. S7 – S11). Data was then extracted from load values after relaxation and fitted to a line from which the slope was calculated. Data is an average of 5 samples and is presented as average ± SD.

2.7. Nanocomposite film formation

PLA was dissolved in dimethylformamide by stirring 4 h at 70 °C at a concentration of 40 mg/mL. To the polymer solution 10% wt/vol CNCs were added and sonicated for 4 h in a bath sonicator adapted with a continuous water flow to avoid sample heating (Sonoswiss SW3H, Sonoswiss AG, Ramsen, Switzerland). Dispersions were then solution casted onto poly(tetrafluoroethylene) Petri dishes and dried in an oven at 70 °C for 3 days to yield 2 g of dried nanocomposite films. The films were then compression moulded 5 min at 140 °C between spacers to achieve a homogenous thickness of 150–200 μm as measured with a caliper. Nanocomposite films of a diameter of 1.2 cm were prepared by punching the films with a stainless steel puncher for cell culture experiments.

2.8. Chondrocyte culture

Human fetal chondrocytes of 2nd passage (primary cells) (Cell Application Inc. San Diego, CA, USA) were cultured in complete expansion medium (chondrocyte growth medium, Cell Application Inc., San Diego, CA, USA) at a density of 10.000–12.000 cell/cm^2 keeping the medium to surface ratio to 0.4 mL/cm^2. The medium was changed every day until 60% confluence was reached, then the volume of the medium was doubled. At 80% confluence cells were subcultured by rinsing them twice with HBSS (Gibco, Life technologies) followed by trypsination for 4 min. Cells were resuspended in 10 mL HBSS, pelleted down by centrifugation at $1.6{\cdot}10^3$ rpm and resuspended in 5 mL expansion medium. Cells were counted in a Neubauer chamber.

2.9. Chondrocyte culture on non-porous films

Neat PLA films and PLA/S–CNC and PLA/P–CNC nanocomposites films were prepared as described above and cut into half circles of 1.2 cm diameter (note that cells attach to both sides of the film), cleaned in 70% EtOH for 15 min and placed directly into 24-well plates (6 repetitions of each sample). Films were rinsed 3 times with expansion medium to eliminate any remnant of ethanol. Adequate aliquots of cell suspension were added on top of the films to reach a density of 10,000–12,000 cells/cm^2. Negative controls were directly cultured on 4-well microcopy culture slides (BD Biosience) to compare cell morphology and viability. After 48 h of culture, polymer films were transferred to new 24-well plates (to avoid interferences of substrate attached cells). After 7 d of culture in expansion medium the cells in controls reached 80% confluence.

2.10. Lactate dehydrogenase (LDH) release and Bicinchoninic acid (BCA) assay

Cells were cultured as explained above and the day before 80% confluence was reached, 100 μL of 0.2% Triton X-100 were added to the medium for the positive control; also, 6 wells were filled up with medium (color change over time used as background). At confluence (7 days), medium of all the different polymer samples as well as positive and negative control, i.e. cells grown on microscopy culture slides, was collected. LDH assay was performed for each sample in triplicate (with 6 samples/substrate type), following manufacturer instructions.

The cells were trypsinized (0.5 mL/well, 4 min), recovered in HBSS and transferred to Eppendorf tubes. The cell suspensions were then centrifuged ($1.6 \cdot 10^3$ rpm, 5 min), supernatant was removed and the cells resuspended in 200 μL PBS. The cells were lysated by quickly freezing and thawing three times in liquid nitrogen. Suspension was centrifuged ($1.6 \cdot 10^3$ rpm, 5 min) and the supernatant was transferred to a new Eppendorf tube. The protein content was measured for each sample in triplicate (6 samples/substrate type) from a 50 μL volume, following manufacturer instructions. The protein concentration was calculated from a standard curve and the ratios to the negative control were calculated and used to normalize the LDH release measurements as cells on different substrates have a different proliferation rate. The experiments were repeated 3 times and data are expressed as mean ± SD.

2.11. Evaluation of cell morphology and viability

After regular culture on non-porous polymer films and at 80% confluence of the negative control (7 d), 3 samples of each condition were used for morphological examination and the other 3 for cell viability studies. For morphological observations, samples were harvested; the culture medium was removed and the samples were rinsed with 1× HBSS three times. The samples were then fixed in 4% paraformaldehyde/PBS solution (Gibco, Life technologies) (15 min, RT) and rinsed in 1× PBS. Cell permeabilization was done by adding 0.2% Triton X-100/PBS solution (15 min, RT). These samples were rinsed again with PBS and covered with 100 μL of the staining solution (5 μL of DAPI, at a concentration of 1 μg/mL, Sigma–Aldrich), 10 μL of Alexa 488-Phalloidin (1:100, Molecular Probes, Life Technologies Europe and 485 μL of 0.2% Triton X-100/PBS). The cells were stained for 1 h in a humid, dark chamber. Finally, samples were rinsed three times with PBS and embedded between 2 coverslips using Pertex® as mounting medium. These samples were stored at 4 °C until usage.

For cell viability studies a propidium iodide (PI) (1 mg/mL, Sigma–Aldrich) solution in water was freshly prepared to reach a concentration of 0.02 mg/mL. A stock solution of fluorescein diacetate (FDA) (Sigma–Aldrich) of 25 mg/mL in acetone was diluted before each experiment to reach a concentration of 0.02 mg/mL in water. Both solutions were mixed in a PI: FDA ratio of 3:1. Cells were rinsed with HBSS and 500 μL of the staining solution were added. After an incubation period of 10 min, cells were rinsed again with HBSS and pictures were recorded within 15 min. A minimum of 5 pictures per sample were recorded (15 pictures/substrate type). Thus, more than 400 cells per experiment were counted. Experiments were repeated 3 times and data are expressed as mean ± SD.

2.12. Laser scanning microscopy

Samples were visualized with an inverted laser scanning microscope Zeiss LSM 710 Axio Observer Z1 equipped with HeNe 633 nm and Ar 488 nm lasers and a 405 nm diode.

2.13. Chondrocyte culture in scaffolds

Single- and multi-layered scaffolds were prepared as described above. Cylindrical scaffolds of 8 mm diameter and ∽ 5 mm thickness were sterilized by immersion in 70% ethanol for 1 h after the samples were placed immediately in 24-well plates and rinsed three times with medium, leaving the samples overnight in the incubator to let any remnant of ethanol evaporate. Chondrocytes from the 2nd passage were harvested counted and a concentrated dispersion of $3 \cdot 10^6$ cell/mL of medium was prepared. Samples were placed on a 6-well plate covered with ethanol incubated parafilm® to create a hydrophobic surface and cells were seeded at $3 \cdot 10^6$ cell/cm^3 density with a syringe (21 gage needle). Scaffold/cell samples were left incubating 4 h to let cells attach and diffuse through the material. Scaffolds were then transferred to 24-well plates and seeded with 2 mL of expansion medium. Medium was changed every two days. Samples were prepared in sextuples.

2.14. Chondrocyte culture in alginate beads

Cells were embedded in alginate beads following a well-established protocol [29]. A dispersion of $2 \cdot 10^6$ cell/mL of alginate solution (1.25% alginic acid sodium salt, 20 mM 2-[4-(2-hydroxyethyl)piperazin-1-yl]ethanesulfonic acid (HEPES) and 150 mM NaCl, pH 7.4) and aspirated with a 21-gauge needle. The dispersion was then added drop-wise into a polymerization solution consisting of 102 mM $CaCl_2$ and 10 mM HEPES at pH 7.4. Alginate beads containing chondrocytes were left polymerizing for 5 min under continuous stirring. Then the solution was filtered into a 50 mL tube using a 40 μm cell strainer (Falcon, BD). Cells were recovered with a spatula and transferred to a 0.9% NaCl solution to wash them for 2 min. This step was repeated three times and in a last step alginate beads were rinsed in complete expansion medium. Finally, the beads were transferred to a Petri dish where the cells were cultured for 2 and 4 weeks under the same conditions as the scaffolds. Dissolution of the beads was performed by immersing the beads (∽200 μL/bead) into a solution containing of 55 mM 2,2′,2″,2‴-(Ethane-1,2-diyldinitrilo) tetraacetic acid (EDTA) and 10 mM HEPES at pH 7.4. After 5 min incubation period the solution was centrifuged and the cells recovered as a pellet.

2.15. Histological evaluation

After two and four weeks of culture, scaffolds were harvested and rinsed three times with HBSS prior to overnight fixation in 4% paraformaldehyde. Samples were then cut longitudinally, rinsed with HBSS and dehydrated by a 14 h program through a series of solutions of 70, 80, 95 and 100% ethanol, xylene and paraffin. Samples were finally embedded in paraffin and microtomed in 10 μm slices that were mounted in microscopy glass slides. Staining with safranin-O was done following supplier's instructions (IHC World). Samples were prepared in triplicate and observed on an optical microscope (Olympus BX51) equipped with linear polarizers (Olympus U-POT) that were crossed and used to identify cellulose nanocrystals inside cartilage tissue slices.

2.16. Real-time polymerase chain reaction (RT-PCR)

After two and four weeks of culture, scaffolds were harvested and total RNA was extracted by freeze–milling and purified using the RNeasy Plus Universal Midi and Mini Kit (Qiagen) for tissue and monolayer cultures, respectively. Extracted total RNA yield was measured photometrically on a NanoDrop 2000 and quantified by measuring the absorbance at 260 nm and 280 nm (relative to absorption at 340 nm). Reverse transcription was performed by

incubating the total RNA samples 1 h at 37 °C with the Omniscript Reverse Transcription Kit (Qiagen); 25 μg of RNA, 1 μL buffer RT (Qiagen), 1 μL of 10 μM Oligo-dT primers (Qiagen), 10 units of RNase inhibitor (RNasin Plus RNase inhibitor, Promega AG, Switzerland), 2 units of Omniscript Reverse Transcriptase (Qiagen) and 1 μL of 5 mM of each dNTP (Qiagen). RT-PCR was carried out by using a Fast SYBR-Green master mix (Applied Biosystems, Life Technologies Europe) with 50 nM primer mix on a total volume of 11 μL, containing 2 μL of ten-fold diluted cDNA. The reaction was carried out on a Fast real-time PCR system (Applied Biosystems) with a program of 20 s denaturation at 95 °C followed by 40 cycles of 30 s at 95 °C and 30 s at 60 °C. The house-keeping gene glyceraldehyde 3-phosphate dehydrogenase (GAPDH) was used as reference to determine the expression of collagen I and collagen II using the $^{\Delta}$Ct method explained previously [30]. Primer sequences (Microsynth AG) were for GAPDH: forward 5′-AAC AGC CTC AAG ATC ATCAGC-3′, reverse 5′- GGATGA TGT TCT GGA GAG CC-3′; for collagen I: forward 5′-GCA ACA GCC GCT TCA CCT AC-3′; reverse 5′-CCA CAT CGA TGA TGG GCA GG-3′; and for collagen II: forward 5′-CAA CAC TGC CAA CGT CCA GAT-3′ and reverse 5′-CTG CTT CGT CCA GAT AGG CAA T-3′. Data is shown as the mean ± SD.

3. Results

3.1. Scaffold fabrication and characterization

The multilayer nanocomposite scaffold was designed to mimic the native mature articular cartilage in orientation and ECM components (Fig. 1). All three layers contain poly(D,L-lactide) (PLA) with a D:L ratio of 89:11, a largely amorphous biopolymer that has been widely used for tissue engineering purposes [31]. This particular grade of amorphous PLA was chosen on account of its biocompatibility, mechanical properties and degradation on-set that will vary from 1 to 4 months [32]. Although a deeper study on the PLA degradation under the specific conditions experienced during cartilage regeneration might be needed, this material appears a priori to be a good candidate of a polymer whose degradation rate matches the tissue regeneration rate.

Chemical cues that emulate the ECM environment and potentially tune the cell phenotypic state were incorporated in the form of cellulose nanocrystals (CNCs) [33,34] that carry a small number of sulfate (S–CNCs, 98.5 ± 8.2 mmol/kg) or phosphate (P–CNCs, 10.1 ± 1.6 mmol/kg) ester groups on their surface (Supporting information Fig. S1). The dimensions of the nanocrystals were determined to be 200 ± 54 nm in length and 25 ± 4 nm in diameter for S–CNCs and 199 ± 56 nm and 23 ± 5 nm for P–CNCs (Supplementary Fig. S2). These crystalline, rod-shaped nanoparticles were further chosen on account of their mechanical reinforcing capability (*vide infra*), their demonstrated ability to support the growth of multiple cell lines [35], and the possibility to easily change their surface chemistry [36], in this particular case, via different one-step isolation procedures. CNCs have been reported to be non-biodegradable under *in vivo* conditions [35]. Upon degradation and bioabsorption of the PLA, CNCs may be expected to be integrated into the generated neocartilage. Since CNCs exhibit a low toxicity to a variety of cell types, a similar behavior is expected in cartilage.

Porous layers based on these components were prepared by thermally induced phase separation (TIPS) methods designed to produce anisotropic (solid–liquid TIPS) [27] or isotropic (liquid–liquid TIPS) [28] porous structures.

Using solid–liquid TIPS, an anisotropic superficial layer with tubular pores was made from PLA only. This layer was designed to mimic the collagen and chondrocyte orientation of the superficial zone of articular cartilage and to guide cell growth and ECM deposition along the direction of its elongated pores arranged parallel to the surface/subchondral bone. Scanning electron microscopy (SEM) images reveal a pore diameter of 45 ± 18 μm and suggest that the pores are interconnected (Fig. 2a).

An isotropic porous layer comprising PLA and 10% w/w S–CNCs, made by liquid–liquid TIPS, emulated the middle zone of articular cartilage, which displays a spherical chondrocyte morphology and disordered ECM. The latter is dominated by a high concentration of sulfated glycosaminoglycans (GAGs) [37], which were thought to be well-represented by S–CNCs. SEM micrographs of this middle layer reveal a cellular structure with slightly elongated pores (71 ± 12 × 50 ± 7 μm, Fig. 2a). Confocal laser scanning microscopy of a reference material made in identical manner with components that had been labeled with fluorescent dyes reveals that the S–CNCs reside primarily at the pore wall surface (Fig. 2a). This architecture appears to result from the phase separation between organic solvent and water during the TIPS process and is desirable as the S–CNCs are meant to guide the cell growth.

A third “deep” layer with tubular pores oriented orthogonal to the subchondral bone was fabricated from PLA and 10% w/w P–CNCs using solid–liquid TIPS. This structure mimics the orientation of collagen and chondrocytes in the deep calcified zone of articular cartilage. Here, the P–CNCs phosphate surface groups were selected to promote the formation of hydroxyapatite. SEM images confirm the desired morphology, revealing interconnected tubular pores with a diameter of 30 ± 6 μm (Fig. 2a), while confocal laser scanning microscopy of a fluorescent reference material revealed that the P–CNCs are homogeneously distributed (Fig. 2a). As a consequence, less phosphate groups are presented to cells in the deep layer than in the middle layer, where sulfate groups are located at the pore wall surface.

The three individual layers were assembled into a multi-layered template using a solvent-assisted bonding approach. This approach is based on the solvent-assisted welding of the individual layers that was achieved via solvent impregnation. The high volatility of the solvent used allowed for a localized dissolution of the PLA at the surfaces, and rapid solidification after an intimate contact between the individual layers had been achieved. This permitted the formation of a continuous interface between the layers and a mechanically coherent structure. The multilayer scaffold was designed to display a total height of ∽5 mm and a diameter of 8 mm; deep and middle layers both had a thickness of ca. 2.4 mm, whereas the superficial layer was only 0.2 mm thick. SEM images (Fig. 2b) show that the interfaces are seamless, that is, the various porous structures are interconnected, allowing for cell and nutrient transport throughout the template.

3.2. Localized hydroxyapatite growth

The scaffold's ability to promote *localized* hydroxyapatite (HAp) formation was explored by separately incubating the three layers for 3 days in $CaCl_2$ and subsequently 7 days in 1.5× concentrated simulated body fluid (SBF). In the case of the PLA/P–CNC deep layer, SEM images (Fig. 2c) show the development of a granulated surface with features that have dimensions of the order of 0.6–1.2 μm (Supplementary information Fig. S3) and are indicative of HAp formation. This was further confirmed by backscattered electron imaging and energy dispersive X-ray (EDX) spectroscopy; the latter shows large amounts of Ca and P and a Ca/P ratio of 1.6 ± 0.1, which is characteristic of HAp in human bone (Fig. 2d) [38]. A Ca/C ratio of >14 suggests that the surface is fully coated with HAp. Gratifyingly, the PLA superficial layer did not show any mineralization, as revealed by backscattered images (Fig. 2d) and a Ca/C ratio of <0.1. The PLA/S–CNC middle layer shows a very low level of mineralization with a Ca/C ratio of 1.0 ± 0.2 and a Ca/P ratio of 1.9 ± 0.2.

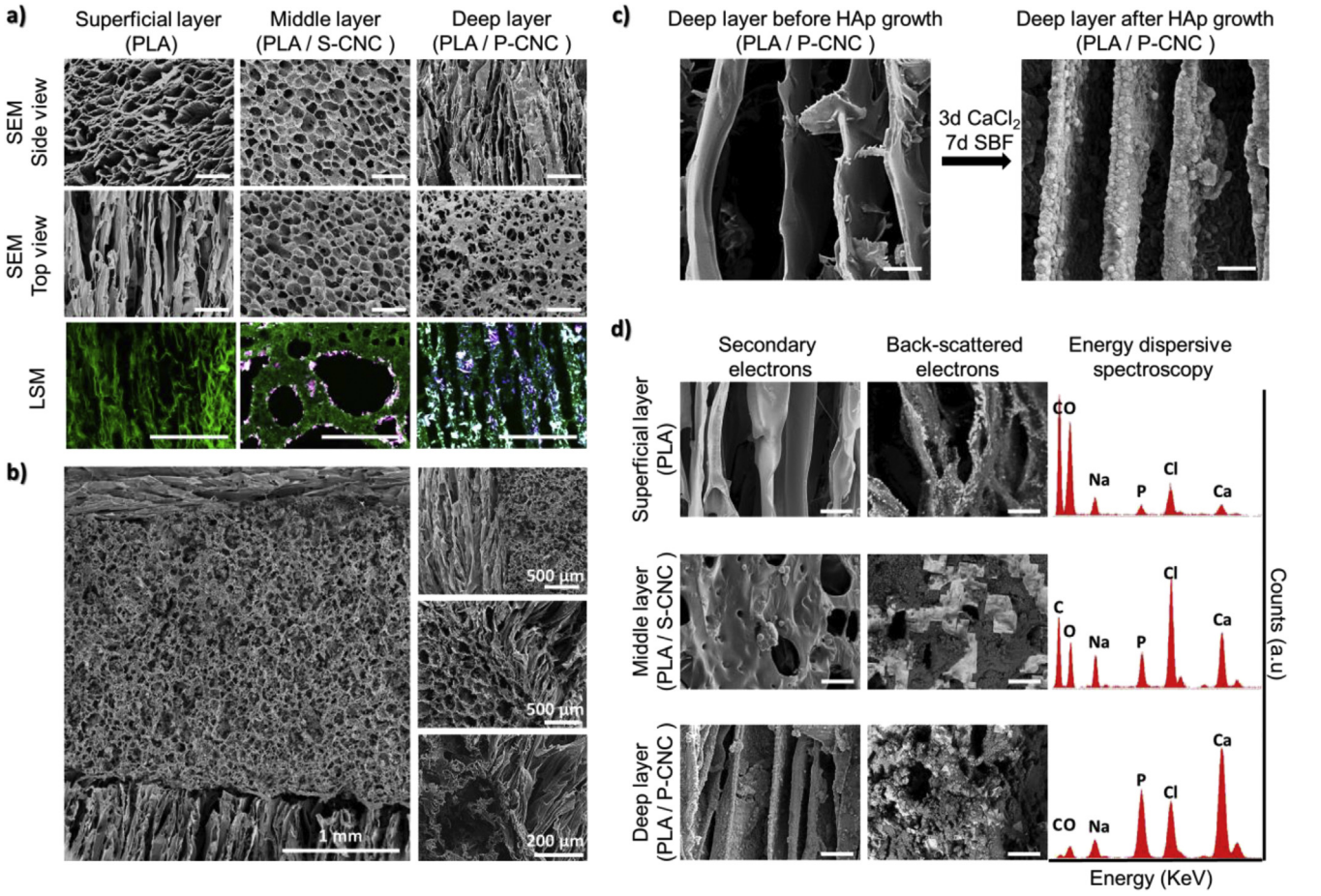

Fig. 2. Morphology and biomineralization of the tissue engineering scaffold. a, Scanning electron microscopy (SEM) images of the different scaffold layers in top and side views, which confirm the targeted morphologies as shown in Fig. 1. Laser scanning microscopy (LSM) images reveal the location of Rhodamine-labeled fluorescent CNCs (pink) and Alexa 488-labeled PLA (green) within the layers and show that in the middle layer, CNCs reside preferably at the pore walls, whereas CNCs in the deep layer are randomly distributed within the PLA. Scale bar is 200 µm in all the images. b, SEM images of the multilayer scaffold after assembly and magnifications of the porous interfaces, which allow for transport of cells and nutrients. c, SEM images of the deep layer before and after hydroxyapatite (HAp) growth via exposure to $CaCl_2$ and simulated body fluid (SBF). Scale bar is 10 µm d, SEM images acquired by detecting secondary electrons (to reveal the morphology) or backscattered electrons (to highlight compositional variation) and energy dispersive spectroscopy (EDS) data of all layers after exposure to $CaCl_2$ (3 d) and SBF, showing the formation of hydroxyapatite (Ca/P ≈ 1.6–1.7) only in the deep layer. Scale bar is 20 µm.

Moreover, a high concentration of chlorine was measured, with Ca/Cl ratios of ~0.1. The back-scattered electron images show the appearance of squared features that resemble those of sodium chloride.

3.3. Mechanical characterization of single and multilayer scaffolds

The mechanical properties of the three individual layers and the multilayer scaffold were probed by compression testing in phosphate buffered saline (PBS) after equilibrating the samples for 1 h in the medium. Unconfined and semi-confined equilibrium experiments were performed to determine Young's (E') and aggregate modulus (H_a) in the direction orthogonal to the layer's surface plane (Supporting information Fig. S7). The semi-confined setup consisted of a small silicone chamber in which the sample was encapsulated between a steel filter and a non-porous rigid plate [39], whereas unconfined experiments were conducted with free-standing samples. Creep stress–strain experiments were performed in unconfined non-equilibrium mode. All stress–strain curves recorded (Fig. 3a,b) are characteristic of porous materials and display elastic behavior at low strain, followed by an irreversible linear regime that is interpreted as cell collapse, and a final exponential increase corresponding to densification. As expected, non-equilibrium unconfined stress–strain curves display higher stresses at given strains compared to the semi-confined equilibrium curves. This stiffening effect is a consequence of water entrapment within the scaffold that is pressurized, opposing the applied load [5]. By contrast, equilibrium stress–strain curves represent the stiffness of the porous material after water evacuation.

The compression tests in confined and unconfined modes show that the isotropic PLA/S–CNC middle layer is the stiffest, with a H_a of 0.34 ± 0.01 MPa and an E' of 0.19 ± 0.04 MPa, followed by the oriented PLA/P–CNC deep layer with a H_a of 0.14 ± 0.04 MPa 0 and an E' of 0.07 ± 0.007 MPa. The oriented PLA superficial layer exhibits by far the lowest stiffness, with a H_a of 0.07 ± 0.003 MPa and an E' of 0.008 ± 0.001 MPa (Supporting information Figs. S8 and S9). A comparison of the compressive mechanical properties of porous layers made with the PLA/CNC composites and the neat PLA revealed a significant reinforcing effect of the CNCs (Supporting information Figs. 13 and 14).

The mechanical characteristics of the multilayer constructs are strongly influenced by the superficial (4% of the total scaffold thickness) and deep layers (48% of the total scaffold thickness),

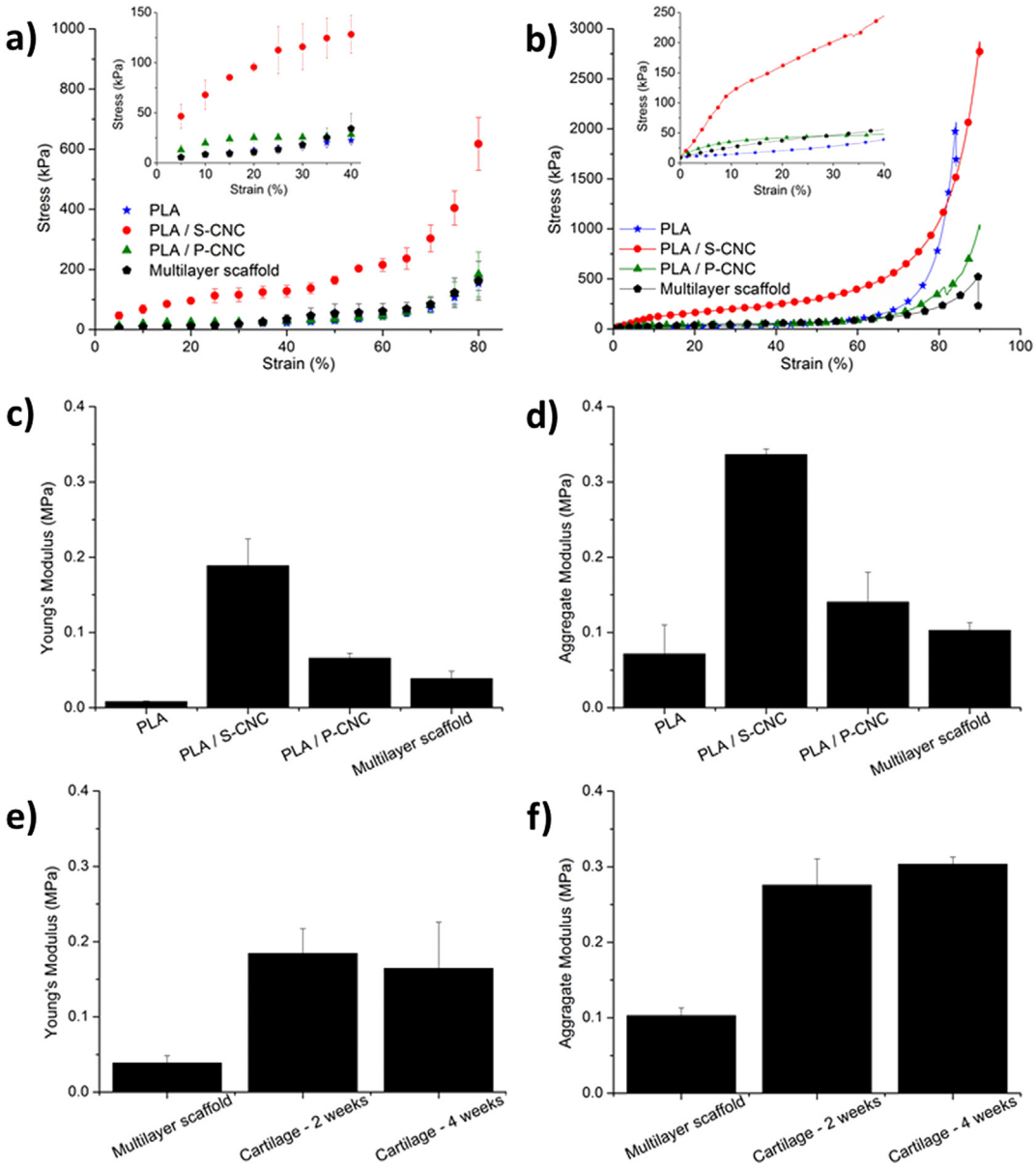

Fig. 3. Compressive properties of the individual layers and multilayer scaffold in PBS (semi-confined and unconfined). a, Stress–strain confined equilibrium creep curves of the single layers and the multilayer scaffold. b, stress–strain unconfined non-equilibrium creep curves of single and multilayer scaffolds. c and d, Young's and aggregate modulus of individual layer and the multilayer scaffold obtained under semi-confined and unconfined modes. e and f, Young's and aggregate modulus of the engineered cartilage after 2 and 4 weeks of culture. Data are presented as average ± SD with n ≥ 3.

leading to an aggregate (multilayer) modulus of 0.1 ± 0.01 MPa and a Young's modulus of 0.04 ± 0.01 MPa (Supporting information Figs. S8 and S9). While the H_a value of the multilayer scaffold is of the same order as that of articular cartilage (0.1–2 MPa [5,37,40–42]), E' of the native tissue (0.3–0.8 MPa [42–45]) is an order of magnitude higher than that of the scaffold.

3.4. Cell viability and cytotoxicity of nanocomposite materials

Prior to engineering tissue using the multilayer scaffolds, the biocompatibility of the three individual layers used was probed by culturing chondrocytes on non-porous films made by solution casting and subsequent compression-moulding the neat PLA, and PLA/P–CNC and PLA/S–CNC nanocomposites containing 10% w/w CNCs, an amount that is identical to the CNC concentration in the porous materials. Polystyrene well plates were used as negative controls to assess the cell viability and morphology, respectively. Chondrocytes that were cultured on neat polymer and nanocomposite films showed the same elongated morphology as the negative control (Fig. 4a) as observed after staining the nucleus and the F-Actin with DAPI (blue) and Phalloidin (green). Furthermore, the cell viability after 7 days of culture, determined by counting alive and death cells in samples stained with propidium iodide (PI, red, death) and fluorescein diacetate (FDA, green, alive), was slightly higher when cultured on either the neat polymer or the nanocomposites but this difference was not statistically significant (Fig. 4a and b). This result may be related to the fact that the PLA and the PLA/CNC nanocomposites display a lower stiffness and a higher water uptake than the polystyrene substrates used for the control [46]. Lactate dehydrogenase (LDH) release to the culture

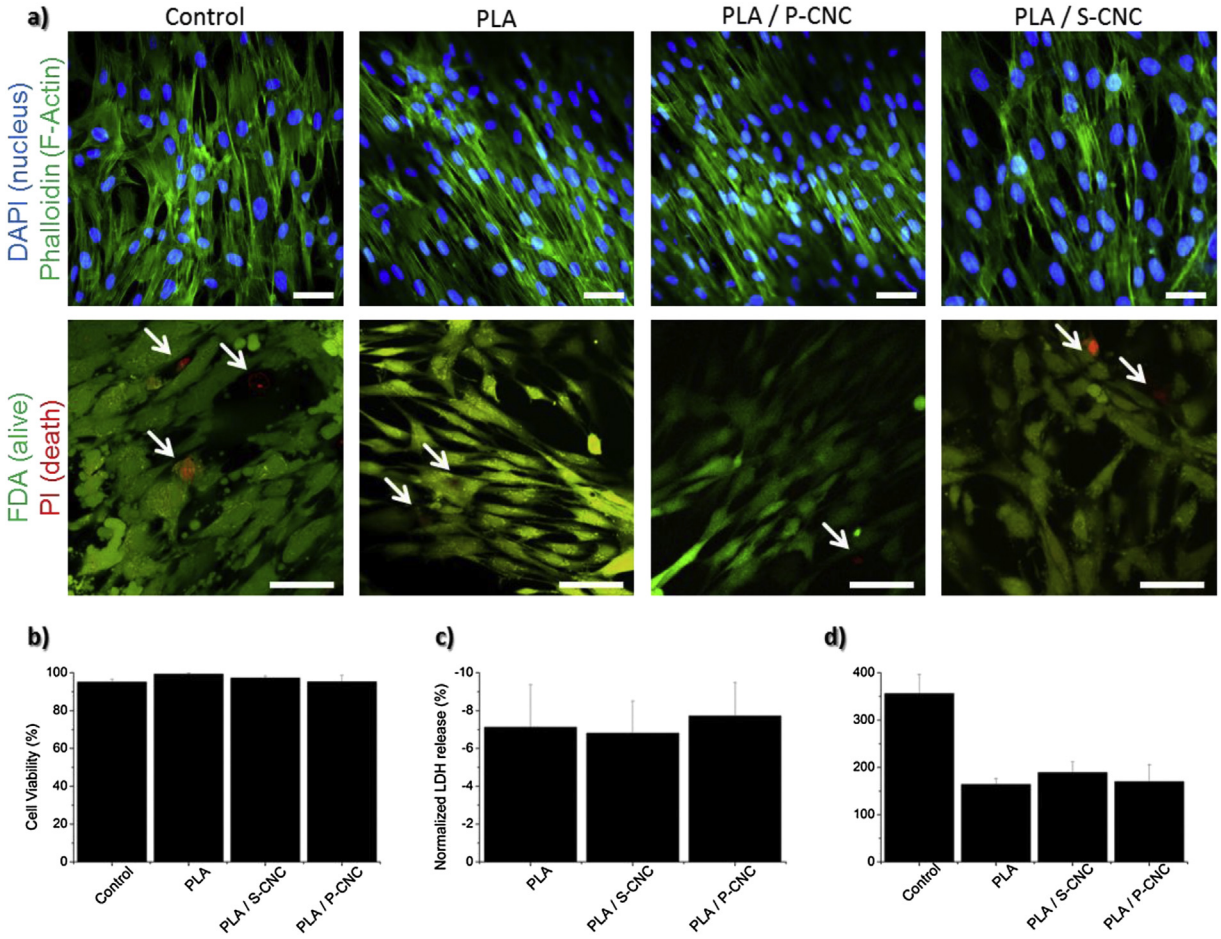

Fig. 4. Influence of substrate type on chondrocyte biocompatibility. a, Laser scanning microscopy (LSM) images of chondrocytes cultured on non-porous films consisting of neat PLA and PLA/S–CNC and PLA/P–CNC nanocomposites as well as polystyrene control (scale bars are 50 μm). Chondrocytes were stained with DAPI (nucleus, blue) and Phalloidin (F-actin, green) for morphology and with prodium iodide (PI) (red, nucleous, death) and fluorescein diacetate (green, membrane, alive) for viability experiments. White arrows point to dead cells (red). The images show no significant differences in cell morphology and viability. The quantification of cell viability (b), normalized LDH release from chondrocytes (c), and protein concentration (d) of the experiment shown in (a) are also shown. The cultures were examined at 80% confluence of the control (7 d) and data are presented as mean ± SD with n = 6.

medium was probed as a measure of cytotoxicity, using cultures in polystyrene 24-well plates treated with Triton X-100 and untreated, as positive (100%) and negative (0%) controls, respectively, and normalizing the data against the protein content, as determined by bicinchoninic acid (BCA) assay, in order to avoid errors from lower cell densities due to different proliferation rates (Fig. 4d). In accordance with the cell viability results, the LDH release of the neat polymer and nanocomposites was 4–7% lower than that of the negative control (Fig. 4c), which confirms the biocompatibility of the materials used.

3.5. *In-vitro tissue formation*

Chondrocytes were cultured in the three individual porous layers and the multilayer scaffold for 2 or 4 weeks, before samples were harvested and analyzed by reverse transcription polymerase chain reaction (RT-PCR) and histological examination. The results show that cells cultured in the individual layers (Fig. 5, three first columns) or in the equivalent layer of the multilayer construct (Fig. 5, left most column) develop in an identical manner, which is indicative of unrestricted transport of cells and nutrients through the interfaces of the multilayer scaffolds. However, as designed, significant differences between the different layer types can be discerned (*vide infra*). Optical microscopy images of microtomed slices of paraffin embedded samples that were collected after 2 weeks and stained with safranin-O (red, specific to proteoglycans) show that tissue growth starts rapidly, but at this end point, large voids can still be observed (Fig. 5). Optical microscopy images acquired after 4 weeks of culture show a much denser cartilaginous tissue with reduced void size, and the color imparted by staining is more intense. The cell morphology after 4 weeks of culture was similar to that observed after 2 weeks, suggesting that no differentiation occurred during culture in the scaffold. Chondrocytes grown in the oriented PLA superficial layer appear to be elongated and well integrated with the scaffold, following its tubular structure. In the case of the isotropic PLA/S–CNC middle layer, optical microscopy images show a clear decrease of the pore size and most intense safranin-O staining relative to culture time. The cells appear to be rounded, likely guided by the morphology of the scaffold and the negative ionic charges imparted by the sulfate groups on the S–CNCs, which in this layer cover the pores' surfaces (*vide supra*). Chondrocytes were also cultured in an isotropic, porous PLA reference scaffold, and in this case an intermediate morphology between elongated and rounded was observed (Fig. S4). This further supports the conclusion that the cell morphology is directed by both, morphology and ionic charges. Chondrocytes

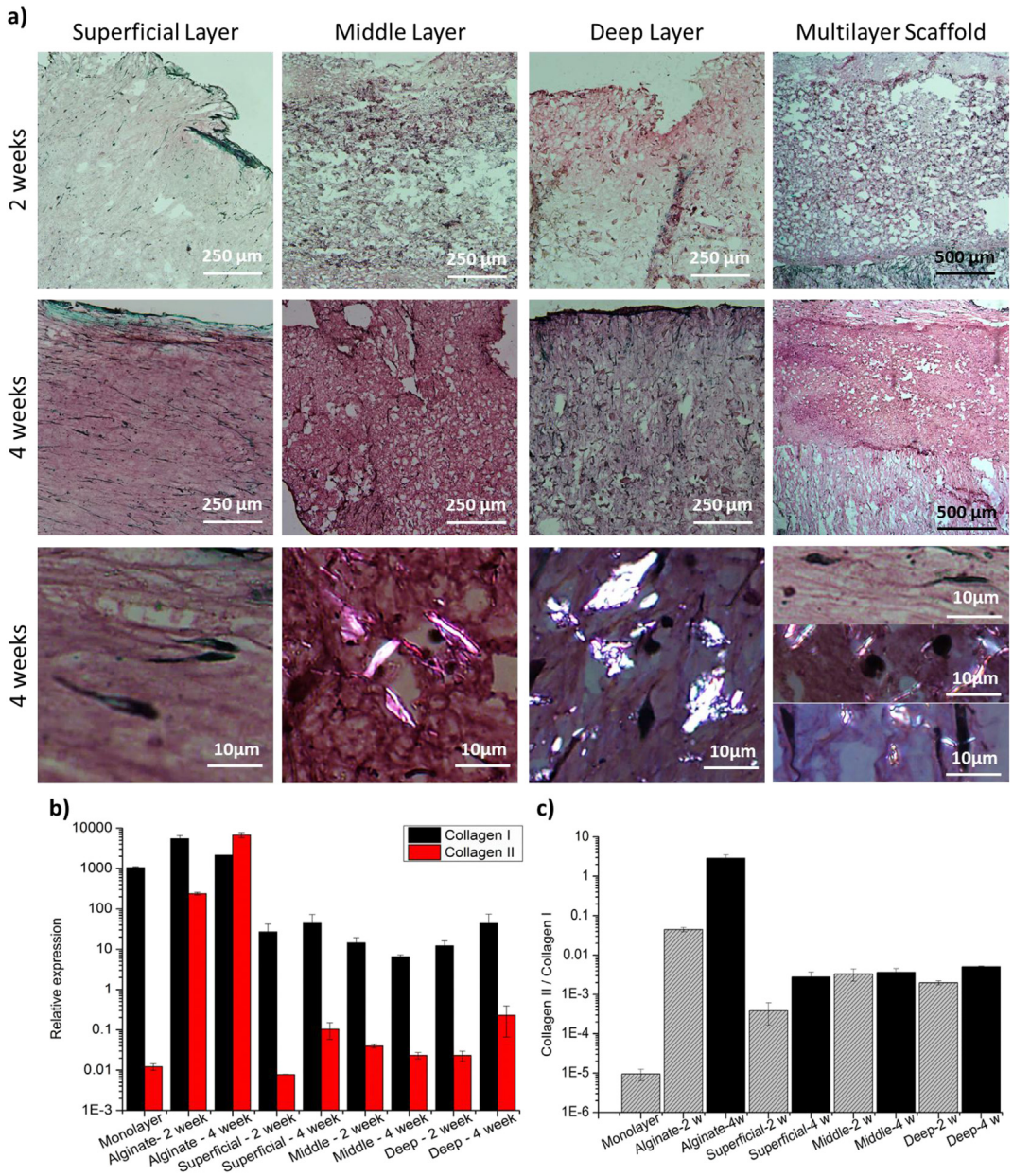

Fig. 5. Cartilage growth in the different layers and the multilayer scaffold. a, Safranin-O staining (with fast green and Weigert's Iron Hematoxylin solutions as counter stains) of 10 µm thick sections of engineered cartilage after 2 and 4 weeks of *in-vitro* culture in individual layers and multilayer scaffolds showing progressive tissue formation upon culture as well as morphological differences of cells cultured in the different layers. b, Plot showing the relative expression levels of collagen II and collagen I after culturing chondrocytes in a monolayer on a polystyrene culture flask, and for 2 and 4 weeks in alginate beads and the superficial, middle and deep layers of the scaffold, respectively (cells were cultured in individual layers). c, Plot showing the collagen II to collagen I ratio in these cultures. Data are presented as average ± SD with n = 3.

cultured on the oriented PLA/P–CNC deep layer, in which P–CNCs are largely buried in the PLA, display an elliptical shape, *i.e.*, a morphology that is in between those of cells grown on the other two layers. Moreover, the tubular structure of the deep layer arranges chondrocytes into a columnar–fashion that is characteristic of the deep zone in mature native cartilage. In all three layers, the cells appear to be well integrated with the scaffold, leading to the formation of neocartilage that features a layered structure, similar to that found in mature cartilage.

The cell differentiation state in the different layers of the scaffold was further evaluated by assessing the ratios of collagen II to collagen I expression levels by RT-PCR, and comparing the values to those of monolayer cultures of chondrocytes on polystyrene culture flasks before their transfer to the scaffolds. Chondrocytes were also cultured under the same conditions in alginate beads, which served an isotropic three-dimensional reference environment that is well-known to cause re-dedifferentiation of dedifferentiated chondrocytes [47]. The collagen II relative expression level increased upon chondrocyte culture in all three layers and alginate beads, as a consequence of the more rounded shape that cells adopt within the scaffolds in comparison to monolayer cultures (Fig. 5). After two weeks of culture, the collagen II relative expression increased from ~0.01 in the monolayer culture on polystyrene to ~0.03 and ~0.02 in the middle and deep scaffolds layers respectively, while the collagen II relative expression of chondrocytes cultured in the superficial layer remained constant. However, chondrocytes cultured

in alginate beads show an increase of 4 orders of magnitude in collagen II relative expression. The collagen II relative expression further increased when cells were cultured for 4 weeks to ∽0.1 and ∽0.2 in the superficial and deep layers and up to ∽$6\cdot10^3$ in the alginate beads, while it remained constant at ∽0.02 in the middle layer. The collagen I expression showed different trends. In all the three layers the collagen I relative expression decreased by two orders of magnitude, while in the alginate beads it showed a 5-fold and 2-fold increase after 2 and 4 weeks of culture, respectively. The evaluation of the collagen II to collagen I relative expression levels, which is commonly used to evaluate the differentiation state of chondrocytes after monolayer culture [48–50], shows clearly that after 4 weeks of culture in the different zones of the new scaffolds, the cells acquire phenotypic states that are different from that of cells cultured in a monolayer. Chondrocytes in the superficial layer appear to have the most dedifferentiated state, as suggested by a collagen II/collagen I expression level ratio of ~$2.7\cdot10^{-3}$, which is three orders of magnitude higher than that of the monolayer cultures. Chondrocytes in the isotropic middle layer account for a collagen II/collagen I ratio of ~$3.6\cdot10^{-3}$, while for the deep layer, a ratio of ~$5.1\cdot10^{-3}$ was measured. Although chondrocytes in the superficial layer appear to be more elongated than in adult native cartilage, this layer is indeed the only one in which collagen I is detected in the native tissue. Hypertrophic chondrocytes in native cartilage (deep zone) have a characteristic elongated shape that is here well resembled but, further analysis of collagen X expression levels would be necessary to clearly assess their phenotypic state. The measured collagen phenotype indicative of re-dedifferentiation of dedifferentiated chondrocytes after monolayer culture is lower than the one observed for other traditional matrices such as alginate, where we measured a collagen II/collagen I ratio of 2.8 ± 0.6 after 4 weeks of culture. Although further analysis of the expression of regulatory factors such as Sox5, Sox6, Sox9 and Runx2 would be interesting, the evolution of the phenotypic state in terms of structural proteins such as collagen II/collagen I expression levels in the superficial, middle and deep layers towards those characteristic of persistent, proliferating and hypertrophic chondrocytes in native cartilage is an effect that, to the best of our knowledge, has not yet being reported for other tissue engineering approaches.

3.6. Mechanical properties of tissue-scaffold constructs

The mechanical characteristics of the engineered tissue-scaffold constructs were studied by confined and un-confined equilibrium compression tests. After tissue engineering, the Young's modulus increased from 0.04 ± 0.01 MPa for the multilayer scaffold to 0.18 ± 0.03 MPa and 0.16 ± 0.06 for the tissue-scaffold construct after 2 and 4 weeks of culture, respectively. A similar behavior is observed for the aggregate modulus, which increased from 0.10 ± 0.01 to 0.28 ± 0.02 MPa after 2 weeks and to 0.30 ± 0.01 MPa after 4 weeks of culture (Supporting information Figs. S10 and S11). Moreover, confined compression curves under equilibrium conditions show the characteristic profile of cartilage, with an initial slope that becomes steeper at ∽30% deformation (Supporting information Fig. S12). We note that at least the moduli of the new tissue-scaffold constructs are comparable to those of mature hyaline cartilage, which is a prerequisite for full mechanical functionality directly upon implantation and may reduce postoperative periods of limited mobility.

4. Conclusions

Taken together, we have demonstrated that the different structural features and chemical cues of the multilayer scaffolds presented here can indeed guide the morphology, orientation, and phenotypic state of cultured chondrocytes so that the engineered tissue emulates the corresponding features of native cartilage. Already after only two weeks of culture, the tissue-scaffold constructs engineered on the basis of the new template displayed Young's and aggregate moduli that are comparable to the values found in mature hyaline cartilage. Furthermore, the possibility to provide a selective anchoring region that connects the soft tissue with the rigid subchondral bone and provides a mechanical gradient via hydroxyapatite growth is an important feature of the multi-functional multi-layer design. However, *in vivo* orthotopic studies in animal models would be required to assess the cartilage regeneration capability of the present tissue-scaffold construct. We note that the design approach utilized here is modular and that the individual components can readily be modified. It appears that chemical cues can be also be imparted through the introduction of small molecules or specific peptide sequences, either in combination with or as alternative to the cellulose nanocrystals employed here, whereas the mechanical properties and degradation rate can be influenced via the choice of the polymeric host.

Acknowledgments

This work was supported by the Swiss National Science Foundation (National Research Programme 64, Project #406440_131264/1) and the Adolphe Merkle Foundation.

Appendix A. Supplementary data

Supplementary data related to this article can be found at http://dx.doi.org/10.1016/j.biomaterials.2015.09.033.

References

[1] D.J. Huey, J.C. Hu, K.A. Athanasiou, Unlike bone, cartilage regeneration remains elusive, Science 338 (2012) 917–921.
[2] L.G. Griffith, G. Naughton, Tissue engineering – current challenges and expanding opportunities, Science 295 (2002) 1009–1014.
[3] J.A. Buckwalter, H.J. Mankin, Articular cartilage repair and transplantation, Arthritis Rheumatism 41 (1998) 1331–1342.
[4] K.A. Athanasiou, E.M. Darling, J.C. Hu, Articular cartilage tissue engineering, Synth. Lect. Tissue Eng. 1 (2009) 1–182.
[5] N.P. Cohen, R.J. Foster, V.C. Mow, Composition and dynamics of articular cartilage: structure, function, and maintaining healthy state, J. Orthop. Sports Phys. Ther. 28 (1998) 203–215.
[6] K. Messner, J. Gillquist, Cartilage repair: a critical review, Acta Orthop. 67 (1996) 523–529.
[7] C. Madeira, A. Santhagunam, J.B. Salgueiro, J.M.S. Cabral, Advanced cell therapies for articular cartilage regeneration, Trends Biotechnol. 33 (2015) 35–42.
[8] I.C. Liao, F.T. Moutos, B.T. Estes, X. Zhao, F. Guilak, Composite three-dimensional Woven Scaffolds with interpenetrating network hydrogels to create functional synthetic articular cartilage, Adv. Funct. Mater. 23 (2013) 5833–5839.
[9] T.G. Kim, H. Shin, D.W. Lim, Biomimetic Scaffolds for tissue engineering, Adv. Funct. Mater. 22 (2012) 2446–2468.
[10] K.S. Furukawa, K. Imura, T. Tateishi, T. Ushida, Scaffold-free cartilage by rotational culture for tissue engineering, J. Biotechnol. 133 (2008) 134–145.
[11] D. Katakai, M. Imura, W. Ando, K. Tateishi, H. Yoshikawa, N. Nakamura, et al., Compressive properties of cartilage-like tissues repaired in vivo with scaffold-free, tissue engineered constructs, Clin. Biomech. 24 (2009) 110–116.
[12] D.W. Hutmacher, Scaffold design and fabrication technologies for engineering tissues – state of the art and future perspectives, J. Biomater. Sci. Polym. Ed. 12 (2001) 107–124.
[13] O. Guillame-Gentil, O. Semenov, A.S. Roca, T. Groth, R. Zahn, J. Voeroes, et al., Engineering the extracellular environment: strategies for building 2D and 3D cellular structures, Adv. Mater. 22 (2010) 5443–5462.
[14] N.H. Dormer, C.J. Berkland, M.S. Detamore, Emerging techniques in stratified designs and continuous gradients for tissue engineering of interfaces, Ann. Biomed. Eng. 38 (2010) 2121–2141.
[15] A.P. Hollander, S.C. Dickinson, W. Kafienah, Stem cells and cartilage development: complexities of a simple tissue, Stem Cells 28 (2010) 1992–1996.
[16] J.M. Dang, K.W. Leong, Natural polymers for gene delivery and tissue engineering, Adv. Drug Deliv. Rev. 58 (2006) 487–499.
[17] S.J. Hollister, Porous scaffold design for tissue engineering, Nat. Mater. 4

(2005) 518–524.
[18] M. Keeney, J.H. Lai, F. Yang, Recent progress in cartilage tissue engineering, Curr. Opin. Biotechnol. 22 (2011) 734–740.
[19] D.W. Hutmacher, Scaffolds in tissue engineering bone and cartilage, Biomaterials 21 (2000) 2529–2543.
[20] J.V. Karpiak, Y. Ner, A. Almutairi, Density gradient multilayer polymerization for creating complex tissue, Adv. Mater. 24 (2012) 1466–1470.
[21] Y. Zhu, H. Wu, S. Sun, T. Zhou, J. Wu, Y. Wan, Designed composites for mimicking compressive mechanical properties of articular cartilage matrix, J. Mech. Behav. Biomed. Mater. 36 (2014) 32–46.
[22] T.B.F. Woodfield, C.A. Van Blitterswijk, J. De Wijn, T.J. Sims, A.P. Hollander, J. Riesle, Polymer scaffolds fabricated with pore-size gradients as a model for studying the zonal organization within tissue-engineered cartilage constructs, Tissue Eng. 11 (2005) 1297–1311.
[23] E.A. Makris, A.H. Gomoll, K.N. Malizos, J.C. Hu, K.A. Athanasiou, Repair and tissue engineering techniques for articular cartilage, Nat. Rev. Rheumatol. 11 (2015) 21–34.
[24] J.R. Capadona, K. Shanmuganathan, D.J. Tyler, S.J. Rowan, C. Weder, Stimuli-responsive polymer nanocomposites inspired by the sea cucumber dermis, Science 319 (2008) 1370–1374.
[25] S. Camarero Espinosa, T. Kuhnt, E.J. Foster, C. Weder, Isolation of thermally stable cellulose nanocrystals by phosphoric acid hydrolysis, Biomacromolecules 14 (2013) 1223–1230.
[26] J. Araki, M. Wada, S. Kuga, T. Okano, Flow properties of microcrystalline cellulose suspension prepared by acid treatment of native cellulose, Colloids Surf. A Physicochem. Eng. Asp. 142 (1998) 75–82.
[27] C. Schugens, V. Maquet, C. Grandfils, R. Jerome, P. Teyssie, Polylactide macroporous biodegradable implants for cell transplantation .2. Preparation of polylactide foams by liquid-liquid phase separation, J. Biomed. Mater. Res. 30 (1996) 449–462.
[28] V. Maquet, A.R. Boccaccini, L. Pravata, I. Notingher, R. Jérôme, Preparation, characterization, and in vitro degradation of bioresorbable and bioactive composites based on Bioglass®-filled polylactide foams, J. Biomed. Mater. Res. Part A 66 (2003) 335–346.
[29] F. Ceuninck, C. Lesur, P. Pastoureau, A. Caliez, M. Sabatini, Culture of Chondrocytes in Alginate Beads, Methods Mol. Med. 100 (2004) 15–22.
[30] T.D. Schmittgen, K.J. Livak, Analyzing real-time PCR data by the comparative CT method, Nat. Protoc. 3 (2008) 1101–1108.
[31] E.J. Caterson, L.J. Nesti, W.-J. Li, K.G. Danielson, T.J. Albert, A.R. Vaccaro, et al., Three-dimensional cartilage formation by bone marrow-derived cells seeded in polylactide/alginate amalgam, J. Biomed. Mater. Res. 57 (2001) 394–403.
[32] P.B. Maurus, C.C. Kaeding, Bioabsorbable implant material review, Operative Tech. Sports Med. 12 (2004) 158–160.
[33] J.M. Dugan, J.E. Gough, S.J. Eichhorn, Directing the morphology and differentiation of skeletal muscle cells using oriented cellulose nanowhiskers, Biomacromolecules 11 (2010) 2498–2504.
[34] D.M. Kalaskar, J.E. Gough, R.V. Ulijn, W.W. Sampson, D.J. Scurr, F.J. Rutten, et al., Controlling cell morphology on amino acid-modified cellulose, Soft Matter 4 (2008) 1059–1065.
[35] N. Lin, A. Dufresne, Nanocellulose in biomedicine: current status and future prospect, Eur. Polym. J. 59 (2014) 302–325.
[36] T. Kuhnt, A. Herrmann, D. Benczedi, E.J. Foster, C. Weder, Functionalized cellulose nanocrystals as nanocarriers for sustained fragrance release, Polym. Chem. 6 (2015) 6553–6562.
[37] R.M. Schinagl, D. Gurskis, A.C. Chen, R.L. Sah, Depth-dependent confined compression modulus of full-thickness bovine articular cartilage, J. Orthop. Res. 15 (1997) 499–506.
[38] P.L. Granja, C.C. Ribeiro, B. De Jeso, C. Baquey, M.A. Barbosa, Mineralization of regenerated cellulose hydrogels, J. Mater Sci. Mater Med. 12 (2001) 785–791.
[39] P. Abdel-Sayed, A. Vogel, M. Nassajian Moghadam, D. Pioletti, Cartilage self-heating contributes to chondrogenic expression, Eur. Cells Mater. 26 (2013) 171–178.
[40] I. Youn, J.B. Choi, L. Cao, L.A. Setton, F. Guilak, Zonal variations in the three-dimensional morphology of the chondron measured in situ using confocal microscopy, Osteoarthr. Cartil. 14 (2006) 889–897.
[41] V.C. Mow, X.E. Guo, Mechano-electrochemical properties of articular cartilage: their Inhomogeneities and Anisotropies, Annu. Rev. Biomed. Eng. 4 (2002) 175–209.
[42] K.A. Athanasiou, M.P. Rosenwasser, J.A. Buckwalter, T.I. Malinin, V.C. Mow, Interspecies comparisons of insitu intrinsic mechanical-properties of distal femoral cartilage, J. Orthop. Res. 9 (1991) 330–340.
[43] R.K. Korhonen, M.S. Laasanen, J. Töyräs, J. Rieppo, J. Hirvonen, H.J. Helminen, et al., Comparison of the equilibrium response of articular cartilage in unconfined compression, confined compression and indentation, J. Biomechanics 35 (2002) 903–909.
[44] J.S. Jurvelin, M.D. Buschmann, E.B. Hunziker, Optical and mechanical determination of poisson's ratio of adult bovine humeral articular cartilage, J. Biomechanics 30 (1997) 235–241.
[45] M.A. Soltz, G.A. Ateshian, Experimental verification and theoretical prediction of cartilage interstitial fluid pressurization at an impermeable contact interface in confined compression, J. Biomechanics 31 (1998) 927–934.
[46] S. Camarero-Espinosa, D.J. Boday, C. Weder, E.J. Foster, Cellulose nanocrystal driven crystallization of poly(d,l-lactide) and improvement of the thermo-mechanical properties, J. Appl. Polym. Sci. 132 (2015) 41607.
[47] H.J. Hauselmann, K. Masuda, E.B. Hunziker, M. Neidhart, S.S. Mok, B.A. Michel, et al., Adult human chondrocytes cultured in alginate form a matrix similar to native human articular cartilage, Am. J. Physiol. Cell Physiol. 271 (1996) C742–C752.
[48] E.M. Darling, K.A. Athanasiou, Rapid phenotypic changes in passaged articular chondrocyte subpopulations, J. Orthop. Res. 23 (2005) 425–432.
[49] P.D. Benya, J.D. Shaffer, Dedifferentiated chondrocytes reexpress the differentiated collagen phenotype when cultured in agarose gels, Cell 30 (1982) 215–224.
[50] M. Jakob, O. Démarteau, D. Schäfer, B. Hintermann, W. Dick, M. Heberer, et al., Specific growth factors during the expansion and redifferentiation of adult human articular chondrocytes enhance chondrogenesis and cartilaginous tissue formation in vitro, J. Cell. Biochem. 81 (2001) 368–377.